Title

Nucleation of metastable aragonite CaCO3 in seawater

Journal

Proceedings of the National Academy of Sciences of the United States of America, 112(11)

ISSN

0027-8424

Authors

Sun, Wenhao

Jayaraman, Saivenkataraman

Chen, Wei

et al.

Publication Date

2015-03-17

DOI

10.1073/pnas.1423898112

Peer reviewed

Nucleation of metastable aragonite $CaCO_3$ in seawater

Wenhao Sun[a], Saivenkataraman Jayaraman[a], Wei Chen[b], Kristin A. Persson[b], and Gerbrand Ceder[a,1]

[a]Department of Materials Science and Engineering, Massachusetts Institute of Technology, Cambridge, MA 02139; and [b]Environmental Energy Technologies Division, Lawrence Berkeley National Laboratory, Berkeley, CA 94720

Edited by David A. Weitz, Harvard University, Cambridge, MA, and approved February 10, 2015 (received for review December 15, 2014)

Predicting the conditions in which a compound adopts a metastable structure when it crystallizes out of solution is an unsolved and fundamental problem in materials synthesis, and one which, if understood and harnessed, could enable the rational design of synthesis pathways toward or away from metastable structures. Crystallization of metastable phases is particularly accessible via low-temperature solution-based routes, such as *chimie douce* and hydrothermal synthesis, but although the chemistry of the solution plays a crucial role in governing which polymorph forms, how it does so is poorly understood. Here, we demonstrate an ab initio technique to quantify thermodynamic parameters of surfaces and bulks in equilibrium with an aqueous environment, enabling the calculation of nucleation barriers of competing polymorphs as a function of solution chemistry, thereby predicting the solution conditions governing polymorph selection. We apply this approach to resolve the long-standing "calcite–aragonite problem"—the observation that calcium carbonate precipitates as the metastable aragonite polymorph in marine environments, rather than the stable phase calcite—which is of tremendous relevance to biomineralization, carbon sequestration, paleogeochemistry, and the vulnerability of marine life to ocean acidification. We identify a direct relationship between the calcite surface energy and solution Mg–Ca ion concentrations, showing that the calcite nucleation barrier surpasses that of metastable aragonite in solutions with Mg:Ca ratios consistent with modern seawater, allowing aragonite to dominate the kinetics of nucleation. Our ability to quantify how solution parameters distinguish between polymorphs marks an important step toward the ab initio prediction of materials synthesis pathways in solution.

nucleation | calcium carbonate | polymorphism | surface energy | solid solution–aqueous solution equilibria

From bulk thermodynamics, one expects the least soluble, most stable crystalline phase to precipitate first from a supersaturated solution. However, for a variety of materials spanning minerals (1), semiconductors (2), and molecular solids (3), the precipitation of the stable phase is either preceded, or totally replaced, by the formation of metastable polymorphs. Although this general phenomenon has been recognized for nearly a century as Ostwald's Rule of Stages (4), it has lacked thermodynamic justification (5), and so Ostwald's rule has served as more of an empirical heuristic than a predictive law. The chemistry of the solution in which precipitation occurs often governs which polymorph forms (6, 7), but the solution does not affect relative bulk stability between crystalline polymorphs. It can, however, influence surface energy at the solvent–crystal interface. Calorimetry experiments with polymorphic oxides have demonstrated that metastable polymorphs can be stabilized at the nanoscale if they have lower surface energy than the stable phase (8, 9). Because nuclei initiate at the nanoscale, this nanoscale stabilization of metastable polymorphs should be intimately related to structure selection during nucleation. Indeed, in addition to being thermodynamically stable at the nanoscale, metastable phases with lower surface energy can surpass the steady-state nucleation rate of the stable phase, provided they have a lower nucleation barrier:

$$\Delta G_c \propto \frac{\gamma^3}{(-RT\ln\sigma)^2}, \quad [1]$$

where γ is the surface energy of the nucleus in the medium, and σ is the supersaturation (10, 11). The steady-state nucleation rate depends exponentially on this nucleation barrier, so minor differences in surface energy between polymorphs can correspond to orders of magnitude differences in nucleation rates, which can potentially compensate for bulk metastability. Quantifying how solution environments modify the relative surface energies between competing polymorphs is therefore foundational to predicting synthesis pathways toward polymorphs with desired materials properties.

Recent high-resolution in situ microscopy techniques have yielded unprecedented observations of nucleation dynamics between competing polymorphs (12, 13), and molecular dynamics simulations of nucleation have identified structural motifs of bulk metastable phases on the surfaces of nuclei for Lennard-Jones solids (14) and ice (15). However, the surface energy of nuclei in solution, and more subtly, the change of surface energy with solution chemistry, has remained inaccessible. In this paper, we use an ab initio thermodynamic framework to directly relate solution chemistry to both the bulk solubility and surface energies of nuclei, allowing us to quantify and compare nucleation rates (Eq. **1**) between competing polymorphs under varying solution parameters, thereby determining polymorph selection as a function of precipitation conditions.

We demonstrate the effectiveness of our approach by resolving one of the oldest examples of crystalline metastability—the precipitation of the aragonite polymorph of calcium carbonate in

Significance

Crystallization from solution is a materials synthesis process common both in nature and in the laboratory. Unlike conventional high-temperature solid-state synthesis, solution-based syntheses often yield metastable phases, contrary to expectations from equilibrium thermodynamics. Using a recently developed ab initio scheme to calculate the surface energy of a critical nucleus in equilibrium with the aqueous environment, we present a framework to compare relative nucleation rates between competing polymorphs as a function of solution chemistry. We apply this approach to demonstrate how seawater chemistry can preferentially bias nucleation toward the metastable aragonite phase of calcium carbonate, rather than the stable phase calcite—which is of great relevance to biomineralization, carbon sequestration, paleogeochemistry, and the vulnerability of marine life to ocean acidification.

Author contributions: W.S., S.J., and G.C. designed research; W.S., S.J., and W.C. performed research; W.S. contributed new methods and analysis tools; W.S., S.J., W.C., K.A.P., and G.C. analyzed data; and W.S., K.A.P., and G.C. wrote the paper.

The authors declare no conflict of interest.

This article is a PNAS Direct Submission.

Freely available online through the PNAS open access option.

[1]To whom correspondence should be addressed. Email: gceder@mit.edu.

This article contains supporting information online at www.pnas.org/lookup/suppl/doi:10.1073/pnas.1423898112/-/DCSupplemental.

seawater instead of the equilibrium phase calcite (16, 17). Because aragonite is metastable with respect to calcite, it has a higher solubility, which has significant implications in biogeochemistry. Oceanic calcium carbonate is the primary CO_2 sink in the global carbon cycle, but for a given p_{CO_2}, aragonite will sequester less carbon than calcite. Furthermore, a substantial fraction of the shells of molluscs, pteropods, and corals are biomineralized aragonite, and its higher solubility renders marine life more vulnerable to increasing ocean acidification (18).

The ratio of Mg^{2+} to Ca^{2+} ions in solution is well-established to be the principal solution parameter in governing calcite–aragonite polymorph selection, where a Mg:Ca ratio >2 yields aragonite (19–21). In fact, alternating deposits of calcite and aragonite in deep-sea calcium carbonate veins have served as evidence for oscillations in ocean Mg:Ca ratios throughout the Phanerozoic Era (22). At high Mg:Ca ratios, such as in modern seawater (Mg:Ca = 5.2), calcite incorporates Mg^{2+}, which is observed to inhibit calcite nucleation and growth, whereas aragonite nucleation is not affected by magnesium in solution (20). The prevailing theory for the inhibition of calcite nucleation is that calcite solubility increases with increasing Mg content in the lattice—reducing its supersaturation at a given $[Ca^{2+}][CO_3^{2-}]$ activity (23, 24). However, this explanation is inconsistent with bulk solubility measurements, which do not find a significant increase in solubility of abiotic Mg–calcite over pristine calcite (25).

In recent reviews and analysis, the possibility of Mg^{2+} modifying the surface energy of calcium carbonate polymorphs has been proposed (9), and the need for a theoretical framework that relates solution–mineral equilibria to surface energy has been emphasized (20). We combine two of our recent methodology developments: (*i*) accurate ab initio predictions of solid–aqueous phase equilibria (26) with (*ii*) efficient calculation and convergence of surface energies (27), to quantify how the solubility and surface energy of calcite and aragonite vary with solution Mg:Ca ratios. We find that the inhibition of calcite nucleation upon Mg^{2+} uptake is primarily due to an increase in surface energy, whereas the increased solubility of Mg–calcite has negligible impact on nucleation rates. Our calculated energetics are used to construct first-principles kinetic phase diagrams, which successfully predict a ratio of Mg:Ca = 2 as a critical boundary for polymorph selection between aragonite and Mg–calcite, and that under modern seawater Mg:Ca ratios, aragonite will nucleate up to 10 orders of magnitude more frequently than calcite. In addition to the importance of these findings to the broad spectrum of scientific disciplines associated with calcium carbonate, the calcite–aragonite problem also serves as an experimentally well-characterized model system to benchmark and validate our theoretical approach to predict and understand competitive nucleation between polymorphs.

Variation of $CaCO_3$ Nucleation Barriers with Solution Mg:Ca Ratio

To evaluate the effect of the solution Mg:Ca ratio on the nucleation barriers of calcite and aragonite, we first require a thermodynamic framework of solution–mineral equilibria that accurately predicts both the equilibrium impurity Mg^{2+} concentration in Mg–calcite, as well as the inertness of aragonite to magnesium in solution. Thermodynamically, it is surprising that calcite incorporates Mg^{2+} from solution at all, as numerous experimental and computational investigations of $CaCO_3$–$MgCO_3$

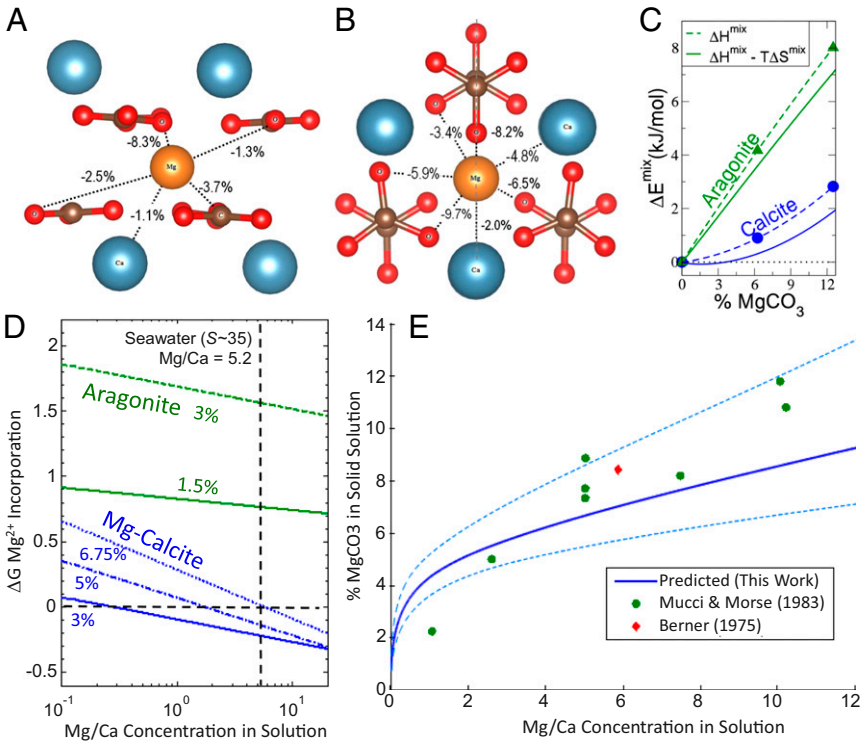

Fig. 1. Structural distortions in the (*A*) calcite and (*B*) aragonite lattices from Mg^{2+} substitution on the Ca^{2+} site. The Ca^{2+} site is ninefold coordinated in aragonite and sixfold coordinated in calcite, resulting in higher enthalpy of mixing of Mg^{2+} in the aragonite structure. (*C*) Calculated solid-state mixing energies of $CaCO_3$–$MgCO_3$. (*D*) Free energy of Mg^{2+} incorporation into $CaCO_3$ in open exchange with aqueous solution of given Mg:Ca ratio. Equilibrium $MgCO_3$ concentration of Mg–calcite corresponds to $\Delta G = 0$. Aragonite is not energetically favorable to incorporate Mg^{2+} at any Mg:Ca ratio. (*E*) Predicted equilibrium $MgCO_3$ concentration in calcite at a given solution Mg:Ca ratio, compared with experiments (23, 25) under similar conditions. Dashed lines correspond to uncertainties in the experimental $\log_{10} K_{sp}^{MgCO_3} = -7.8 \pm 0.3$.

solid solutions have determined positive free energies of mixing in the dilute (<15%) Mg^{2+} regime, suggesting immiscibility (28–31). We note that although previous studies reference the free energies of mixing of $Ca_{1-x}Mg_xCO_3$ against solid-state $CaCO_3$ and $MgCO_3$, pure magnesite $MgCO_3$ is known not to precipitate out of water even under very high supersaturations (32), and so the relevant reaction under this constrained equilibrium should actually be with respect to the aqueous ions (Eq. **2**):

$$x\ Mg^{2+}(aq) + CaCO_3(s) \rightarrow Ca_{1-x}Mg_xCO_3(s) + x\ Ca^{2+}(aq). \quad [2]$$

The Gibbs free energy of this reaction can be evaluated as

$$\Delta G_{Ca_{1-x}Mg_xCO_3} = \Delta H^{mix}_{Ca_{1-x}Mg_xCO_3} - T\Delta S^{mix}_{Ca_{1-x}Mg_xCO_3} + xRT\ln\left(\left(\frac{K_{sp}^{MgCO_3}}{K_{sp}^{CaCO_3}}\right)\left(\frac{a_{Ca^{2+}}}{a_{Mg^{2+}}}\right)\right), \quad [3]$$

where the first two terms are the solid–solid mixing enthalpies and entropies from a standard solid-solution model, but the third term represents the free energy of solution–mineral ion exchange (derivation in *SI Appendix*, section S.I.2). This term is negative when the ratio of Mg:Ca ions in solution is large, and can offset positive solid–solid mixing free energies, resulting in a solution-stabilized impurity concentration of Mg^{2+} in calcite.

Fig. 1*C* shows the calculated free energy of mixing for $CaCO_3$–$MgCO_3$ solid solutions in the dilute $MgCO_3$ limit. In agreement with previous studies, we confirm a positive mixing free energy of Mg^{2+} into calcite solid solution when referenced against solid $CaCO_3$ and $MgCO_3$. Additionally, we report that Mg^{2+} incorporation into aragonite is over 4 times more energetically unfavorable than into calcite. The greater energy cost originates from the difference in oxygen coordination of the divalent cation. In both calcite and aragonite, the smaller Mg^{2+} ion induces a stress field such that the nearest-neighbor Mg–O bond is ∼9% shorter than the corresponding Ca–O bond (Fig. 1 *A* and *B*). However, because the divalent cation is only sixfold coordinated by oxygen in calcite, whereas it is ninefold coordinated by oxygen in aragonite, the energy penalty of Mg^{2+} on Ca^{2+} substitution is far greater in the aragonite structure. Furthermore, Mg^{2+} is almost never observed to be ninefold coordinated in crystals (33).

When the $MgCO_3$ concentration, x, in $Ca_{1-x}Mg_xCO_3$ is in equilibrium with seawater, the free energy for $\Delta G_{Ca_{1-x}Mg_xCO_3}$ in Eq. **3** will be zero. By identifying the critical solution Mg:Ca ratio that compensates for the positive $CaCO_3$–$MgCO_3$ mixing free energies, we successfully predict Mg^{2+} concentrations in Mg–calcite in good agreement with experiments (Fig. 1*C*), obtaining a Mg^{2+} concentration of ∼7% in Mg–calcite at the modern seawater Mg:Ca ratio of 5.2. We further confirm from first principles that the aragonite structure is unable to accommodate Mg^{2+} substitution at any Mg:Ca chemical potential, due to its high enthalpy of incorporation.

Using our first-principles–calculated $CaCO_3$–$MgCO_3$ solid-solution free energies, we first determine the increase in calcite solubility with Mg uptake, to quantify the claim that it is responsible for the inhibition of calcite nucleation. The solubility product for Mg–calcite can be calculated from Eq. **4**:

$$-RT\ln K_{sp}^{Ca_{1-x}Mg_xCO_3} = (1-x)\mu^{\circ}_{Ca^{2+}} + x\mu^{\circ}_{Mg^{2+}} + \mu^{\circ}_{CO_3^{2-}} - \mu_{Ca_{1-x}Mg_xCO_3}. \quad [4]$$

Although $\mu_{Ca_{1-x}Mg_xCO_3}$ is straightforward to obtain from density functional theory (DFT), the standard state chemical potentials of ions in solution can be costly and error-prone to obtain from computation. Instead, we reference the Ca^{2+}, Mg^{2+}, and CO_3^{2-} ion

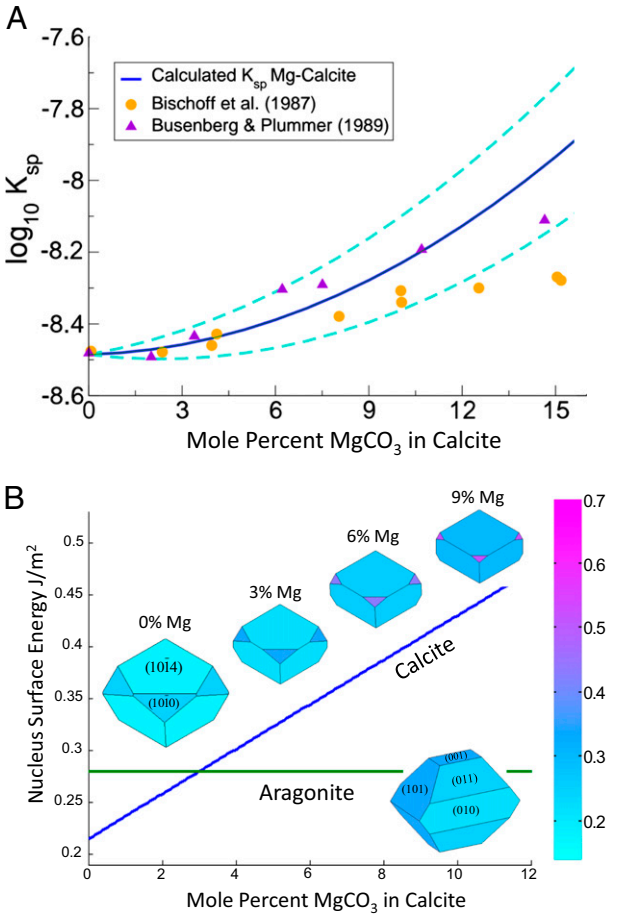

Fig. 2. (*A*) Predicted equilibrium solubility product of Mg–calcite. Dashed lines correspond to different reference states for the aqueous ion formation energies (*SI Appendix*, section S.I.5). (*B*) Morphology-averaged surface energies for hydrated Mg–calcite and aragonite as a function of Mg^{2+} uptake in calcite. Colors correspond to facet-specific surface energies. Aragonite does not incorporate Mg^{2+}.

formation energies to reproduce the experimental $K_{sp}^{calcite}$ and $K_{sp}^{magnesite}$ (derivation in *SI Appendix*, section S.I.5). Combining these referenced ion chemical potentials with the calculated Mg–calcite solid-solution formation energies, we predict a 30% increase of $K_{sp}^{calcite}$ from $10^{-8.48}$ to $10^{-8.36}$ at ∼7% $MgCO_3$, in close agreement with experiment (Fig. 2*A*). This increased solubility reduces the bulk driving force for calcite nucleation by 0.3 RT/mol, which is about an order of magnitude smaller than typical driving forces for nucleation, suggesting that the increased solubility of Mg–calcite plays only a minor role in inhibiting calcite formation.

In contrast, the effect of Mg^{2+} incorporation on the calcite surface energy can drastically inhibit calcite nucleation. Surface energies are obtained from DFT computations of hydrated calcium carbonate surface slabs with partial Mg^{2+} substitution on calcium sites (*SI Appendix*, section S.I.6). The solvated surface is modeled by adsorption of explicit water molecules on the cation sites, which physically captures the thermodynamic effect of water hydration (34). The dominant facets of the aragonite nucleus are predicted to be the (001), (011), (010), and (110) forms, and for calcite the $(10\bar{1}4)$ and $(10\bar{1}0)$ forms, consistent with experimental morphologies and other calculations in the literature (35, 36). We determine the hydrated surface energy of a pristine calcite nucleus to be 0.21 J/m^2, which is lower than that of

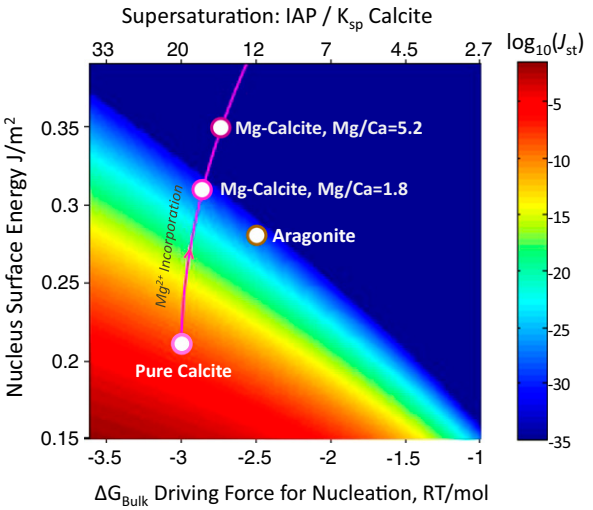

Fig. 3. Dimensionless $\log_{10}$ steady-state nucleation rates of calcium carbonate polymorphs at 25 °C plotted (color-coded) as a function of the nucleus surface energy and the bulk driving force for nucleation. Inhibition of calcite nucleation upon Mg uptake is primarily due to an increase in the surface energy, rather than from a reduction of bulk driving force from increased solubility. Example nucleation rates for aragonite and calcite at given Mg:Ca ratios are plotted at $\sigma = [a_{Ca^{2+}}][a_{CO_3^{2-}}]/K_{sp}^{calcite} = 20$, near the onset of aragonite nucleation.

aragonite, 0.28 J/m^2, confirming that in a solution with no magnesium, both the bulk driving force and the surface energy favors a kinetic preference for calcite nucleation. However, we find that the Mg–calcite hydrated surface energy increases linearly with increasing $MgCO_3$ in calcite solid solution (Fig. 2*B*), a byproduct of the stress-induced energy penalty of bulk Mg^{2+} incorporation, reaching 0.35 J/m^2 at the equilibrium ~7% $MgCO_3$ concentration of Mg–calcite in modern seawater.

Competitive Nucleation Between Aragonite and Mg–Calcite

In Fig. 3, we assess the combined contribution of the surface energy and bulk driving force to the steady-state nucleation rate (color-coded) of the $CaCO_3$ polymorphs. The onset of homogeneous nucleation occurs for nucleation barriers <76 k_BT (37), so for the aragonite surface energy of 0.28 J/m^2 we predict a supersaturation of $\sigma_{calcite} = 18$ to be necessary to initiate nucleation, agreeing quantitatively with experimental observations (38). Calcite will always experience a greater bulk driving force for nucleation than aragonite, by up to $\Delta G_{calcite \rightarrow aragonite} = 0.5$ RT/mol. However, as calcite incorporates Mg^{2+}, its surface energy and solubility increase (purple line), reducing its nucleation rate by many orders of magnitude. Because the nucleation barrier scales as the cube of the surface energy, but is only reduced by the square of $\ln \sigma$ (Eq. **1**), the increase in surface energy plays a much more significant role in inhibiting Mg–calcite nucleation than the increase in solubility.

We collect our findings in a kinetic phase diagram in Fig. 4—a synthesis map of polymorph selection as a function of the solution parameters Mg:Ca ratio and supersaturation. Aragonite nucleates beyond its critical supersaturation of $\sigma_{calcite} = 18$ independent of the solution Mg:Ca ratio. On the other hand, the increase in Mg–calcite surface energy with rising Mg:Ca ratios requires greater supersaturations to trigger calcite nucleation. In solutions with no Mg^{2+}, calcite is the only phase nucleated, initiating at supersaturations as low as $\sigma_{calcite} = 5$. At Mg:Ca = 2, we predict the minimum supersaturation for calcite nucleation to increase to $\sigma_{calcite} = 18$, the same as aragonite, resulting in similar nucleation rates for both polymorphs. At the modern seawater Mg:Ca ratio of 5.2, the supersaturation necessary for calcite nucleation increases to $\sigma_{calcite} = 35$, far greater than what is necessary to nucleate aragonite. For a broad span of supersaturations at this Mg:Ca ratio, aragonite nuclei will form up to 10 orders of magnitude more frequently than calcite nuclei, leaving only the metastable phase present in solution to initiate crystal growth. This predicted synthesis map agrees closely with ones obtained experimentally (21), and is robust with respect to minor errors that may arise from approximations taken during calculation (*SI Appendix*, section S.I.7).

Discussion

Our predicted ab initio synthesis map confirms two long-standing empirical observations: (*i*) that a Mg:Ca ratio ~2 sets an effective boundary for polymorph selection between aragonite and Mg–calcite, where Mg:Ca >2 preferences aragonite, and (*ii*) that under modern seawater Mg:Ca ratios, metastable aragonite dominates the kinetics of nucleation. In addition, we confirm previous findings that a critical supersaturation of 18 is necessary to initiate aragonite nucleation (38). This is surprising, considering that the ocean is only about 4 times supersaturated with respect to aragonite (18). However, this puzzle might be resolved by considering the various polymorphic stages that precede calcite and aragonite in calcium carbonate precipitation. Upon supersaturation, liquid–liquid separations of calcium and carbonate ions form prenucleation clusters (39, 40), which aggregate to become amorphous calcium carbonate (41), which then proceeds via dissolution–reprecipitation reactions to vaterite and finally to either calcite or aragonite (42). We hypothesize that the local $[Ca^{2+}][CO_3^{2-}]$ activity near dissolving transition polymorphs is far greater than the average $[Ca^{2+}][CO_3^{2-}]$ activity in solution, providing the necessary local supersaturations to nucleate the final calcite and aragonite phases.

In this procession of calcium carbonate polymorphs, each phase is lower in energy than the last (43), consistent with the empirical Ostwald's Rule of Stages. The nucleation framework put forth in this paper reinforces a classical nucleation theory-based mechanism for Ostwald's Rule of Stages (10, 11), whose thermodynamic foundations have remained controversial for over a century. For the calcium carbonate polymorphs, bulk metastability, and therefore solubility, is ordered amorphous calcium carbonate (ACC) > vaterite > aragonite > calcite (43). For the more soluble phases to precipitate first, their nucleation barriers, and thus surface energies, must be inversely ordered

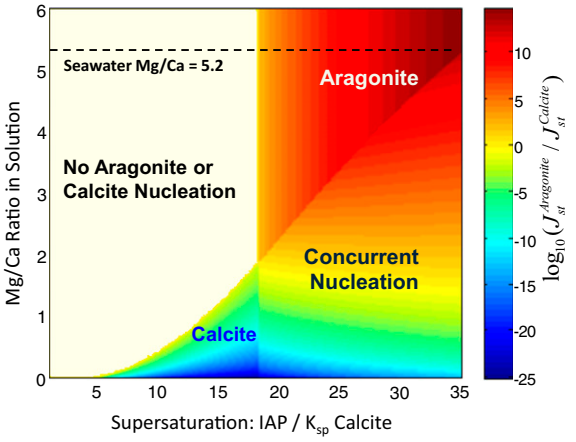

Fig. 4. Kinetic phase diagram of the relative nucleation rate between calcite and aragonite (color-coded) as a function of solution Mg:Ca ratio and the supersaturation. For Mg:Ca = 5.2 (modern seawater) only aragonite is preferred to nucleate. Concurrent nucleation of calcite and aragonite occurs for a broad span of supersaturations near Mg:Ca = 2.

ACC < vaterite < aragonite–calcite. Indeed, molecular dynamics simulations have shown that ACC formation might be barrierless (39), although the nucleation barrier of vaterite is challenging to quantify computationally, due to the complexity of the vaterite structure (44, 45). Nevertheless, such inverse relationships between surface energy and bulk metastability would be consistent with other polymorphic oxides (8). The universality of this observed relationship may originate from the fact that a metastable structure has less cohesive energy than the stable phase, which implies a lower energy of cleavage—e.g., a lower surface energy.

Although our study focuses on calcium carbonate nucleation in inorganic abiotic environments, macromolecule proteins and organic matrices can also influence polymorph selection between calcite and aragonite during crystallization (46, 47). These macromolecules can influence calcium carbonate interfacial energies during heterogeneous nucleation on substrates (48), modify the local Mg^{2+} concentrations around nascent nuclei (49), template polymorph selection epitaxially (50), and influence the selective binding strength of aqueous ions (51). Mg^{2+} also incorporates into the transient prenucleation clusters and amorphous calcium carbonate phases (52), which can be stabilized in the presence of macromolecules (53), and whose dissolution may further alter local Mg^{2+} concentrations from that of the bulk solution. A deeper understanding of how organic and biological entities influence nucleation thermodynamics and kinetics will pave the way toward a mechanistic understanding of polymorph selection during biomineralization.

We have thus established an explanation for the selection of a metastable polymorph in aqueous conditions by studying the energy of its critical nucleus in equilibrium with the aqueous environment. Control of polymorphism is a central goal in materials synthesis, as metastable phases can potentially exhibit superior material properties than their stable counterparts. By identifying surface thermodynamics as a potential handle in crystal structure engineering, we highlight the need for a greater understanding of how the surface energy varies as a function of solvent, substrate, organic and inorganic adsorbates, pH, electrochemical conditions, surface charge, and biological agents. Materials engineers can then apply these insights to design synthesis conditions that drive the surface energy of a desired polymorph below that of competing phases, kinetically biasing crystallization toward desired structures.

Methods

DFT calculations were performed using the Vienna Ab-initio Software Package (VASP) (54). We used the projector augmented wave (55) method with the Perdew–Burke–Ernzerhof (56) generalized-gradient approximation. Plane-wave basis cutoff energies were set at 520 eV for all calculations. Brillouin zones were sampled using Gaussian smearing, with at least 1,000 *k* points per reciprocal atom for bulk unit cells, and at least 700 *k* points per reciprocal atom for surface slabs. Atoms were initially relaxed until forces were 1×10^{-6} eV/Å. All structure preparations were performed using the Python Materials Genomic (pymatgen) package (57).

$CaCO_3$–$MgCO_3$ solid-solution calculations were performed using the supercell approach, substituting Mg onto a Ca site: 6.25% and 12.5% Mg–calcite was calculated on a $2 \times 2 \times 2$ primitive calcite unit cell (16 Ca atoms); 6.25% and 12.5% Mg–aragonite was calculated on a $2 \times 2 \times 1$ conventional aragonite unit cell (16 Ca atoms). For the 6.25% case, all Ca atoms are symmetrically equivalent, so there is only one possible Mg substitution. For 12.5%, the two Mg^{2+} ions were placed as far apart from each other as possible, under periodic boundary conditions.

Surface energy calculations were performed on surface slabs at least 15 Å thick and with 16-Å vacuum, generated using the efficient creation and convergence scheme created by the authors in ref. 27. Hydrated surface energies were calculated with explicit H_2O molecules, placed 2.4 Å above each calcium ion (34), oriented with lone-pair orbitals facing the nearest Ca^{2+} or Mg^{2+} ion and a hydrogen pointed toward the nearest oxygen atom, then relaxed by simulated annealing. The use of H_2O adsorbates is a reasonable approximation for hydrated surface energies under pH values corresponding to neutral and ocean water (pH = 8.1). We attain $\gamma_{\text{hydrated}}/\gamma_{\text{dry}}$ ratios ranging from 50% to 70%, consistent with calorimetry studies on oxides (8) and to previous computational studies on $CaCO_3$ surfaces using COSMIC (COnductor-like Screening MOdel) solvation models (36).

Surface energies were calculated with the equation

$$\gamma = \frac{1}{2A}\left(E_{\text{slab}} - NE_{\text{bulk}} - \sum_i N_i \mu_i\right).$$

For water molecules coming from the liquid phase at 298 K, we use a chemical potential of −14.60 eV per H_2O. This is obtained by calculating in DFT the total energy of the H_2O molecule and subtracting the experimental heat of evaporation at room temperature. To calculate the chemical potentials of the Ca^{2+} and Mg^{2+} aqueous ions, we used the scheme from ref. 26, using CaO and MgO as the reference solids.

ACKNOWLEDGMENTS. W.S. thanks Shirley Y. Chan for helpful discussions. This work was supported by the US Department of Energy, Office of Basic Energy Sciences, under Contract DE-FG02-96ER45571, and the National Science Foundation Graduate Research Fellowship (to W.S.). Computing resources were provided by the National Energy Research Scientific Computing Center, as well as by the Center for Functional Nanomaterials, Brookhaven National Laboratory, which is supported by the US Department of Energy, Office of Basic Energy Sciences, under Contract DE-AC02-98CH10886. Work at the Lawrence Berkeley National Laboratory was supported by the Assistant Secretary for Energy Efficiency and Renewable Energy, under Contract DE-AC02-05CH11231. The Materials Project work is supported by US Department of Energy, Office of Basic Energy Sciences program under Grant EDCBEE.

1. Morse JW, Casey WH (1988) Ostwald processes and mineral paragenesis in sediments. *Am J Sci* 288(6):537–560.
2. Washington AL, 2nd, et al. (2012) Ostwald's Rule of Stages and its role in CdSe quantum dot crystallization. *J Am Chem Soc* 134(41):17046–17052.
3. Rodríguez-Hornedo N, Murphy D (1999) Significance of controlling crystallization mechanisms and kinetics in pharmaceutical systems. *J Pharm Sci* 88(7):651–660.
4. Ostwald W (1897) Studien uber die Bildung und Umwandlung fester Korper. *Z Phys Chem* 22:289–330.
5. Hedges LO, Whitelam S (2011) Limit of validity of Ostwald's rule of stages in a statistical mechanical model of crystallization. *J Chem Phys* 135(16):164902.
6. Stein A, Keller SW, Mallouk TE (1993) Turning down the heat: Design and mechanism in solid-state synthesis. *Science* 259(5101):1558–1564.
7. Gopalakrishnan J (1995) Chimie douce approaches to the synthesis of metastable oxide materials. *Chem Mater* 7(7):1265–1275.
8. Navrotsky A (2011) Nanoscale effects on thermodynamics and phase equilibria in oxide systems. *ChemPhysChem* 12(12):2207–2215.
9. Navrotsky A (2004) Energetic clues to pathways to biomineralization: Precursors, clusters, and nanoparticles. *Proc Natl Acad Sci USA* 101(33):12096–12101.
10. Stranski IN, Totomanow D (1933) Rate of formation of (crystal) nuclei and the Ostwald step rule. *Z Phys Chem* 163:399–408.
11. Baumgartner J, et al. (2013) Nucleation and growth of magnetite from solution. *Nat Mater* 12(4):310–314.
12. Nielsen MH, Aloni S, De Yoreo JJ (2014) In situ TEM imaging of $CaCO_3$ nucleation reveals coexistence of direct and indirect pathways. *Science* 345(6201):1158–1162.
13. Kimura Y, Niinomi H, Tsukamoto K, García-Ruiz JM (2014) In situ live observation of nucleation and dissolution of sodium chlorate nanoparticles by transmission electron microscopy. *J Am Chem Soc* 136(5):1762–1765.
14. ten Wolde PR, Ruiz-Montero MJ, Frenkel D (1995) Numerical evidence for bcc ordering at the surface of a critical fcc nucleus. *Phys Rev Lett* 75(14):2714–2717.
15. Russo J, Romano F, Tanaka H (2014) New metastable form of ice and its role in the homogeneous crystallization of water. *Nat Mater* 13(7):733–739.
16. Fyfe WS, Bischoff JL (1965) The calcite-aragonite problem. *Spec Publ - Soc Econ Paleontol Mineral* 13:3–13.
17. Leitmeir H (1910) Zur kenntnis der Carbonate: I. Die Dimorphie des kohlensauren Kalkes. *Neues Jahrb Mineral* I:49–74.
18. Orr JC, et al. (2005) Anthropogenic ocean acidification over the twenty-first century and its impact on calcifying organisms. *Nature* 437(7059):681–686.
19. Morse JW, Wang Q, Tsio MY (1997) Influences of temperature and Mg:Ca ratio on CaCO3 precipitates from seawater. *Geology* 25(1):85–87.
20. Morse JW, Arvidson RS, Lüttge A (2007) Calcium carbonate formation and dissolution. *Chem Rev* 107(2):342–381.
21. De Choudens-Sánchez V, González LA (2009) Calcite and aragonite precipitation under controlled instantaneous supersaturation: Elucidating the role of $CaCO_3$ saturation state and Mg/Ca ratio on calcium carbonate polymorphism. *J Sediment Res* 79(6):363–376.
22. Coggon RM, Teagle DA, Smith-Duque CE, Alt JC, Cooper MJ (2010) Reconstructing past seawater Mg/Ca and Sr/Ca from mid-ocean ridge flank calcium carbonate veins. *Science* 327(5969):1114–1117.
23. Berner RA (1975) The role of magnesium in the crystal growth of calcite and aragonite from sea water. *Geochim Cosmochim Acta* 39(4):489–504.

24. Davis KJ, Dove PM, De Yoreo JJ (2000) The role of Mg2+ as an impurity in calcite growth. *Science* 290(5494):1134–1137.
25. Mucci A, Morse JW (1984) The solubility of calcite in seawater solutions of various magnesium concentration, It= 0.697 m at 25 C and one atmosphere total pressure. *Geochim Cosmochim Acta* 48(4):815–822.
26. Persson KA, Waldwick B, Lazic P, Ceder G (2012) Prediction of solid-aqueous equilibria: Scheme to combine first-principles calculations of solids with experimental aqueous states. *Phys Rev B* 85:235438.
27. Sun W, Ceder G (2013) Efficient creation and convergence of surface slabs. *Surf Sci* 617:53–59.
28. Bischoff WD (1998) Dissolution enthalpies of magnesian calcites. *Aquatic Geochem* 4(3-4):321–336.
29. Burton BP, Van de Walle A (2003) First-principles-based calculations of the $CaCO_3$–$MgCO_3$ and $CdCO_3$–$MgCO_3$ subsolidus phase diagrams. *Phys Chem Miner* 30(2):88–97.
30. Elstnerová P, et al. (2010) Ab initio study of thermodynamic, structural, and elastic properties of Mg-substituted crystalline calcite. *Acta Biomater* 6(12):4506–4512.
31. Vinograd VL, Burton BP, Gale JG, Allan NL, Winkler B (2007) Activity–composition relations in the system $CaCO_3$–$MgCO_3$ predicted from static structure energy calculations and Monte Carlo simulations. *Geochim Cosmochim Acta* 71(4):974–983.
32. Xu J, et al. (2013) Testing the cation-hydration effect on the crystallization of Ca-Mg-CO_3 systems. *Proc Natl Acad Sci USA* 110(44):17750–17755.
33. Brown ID (1988) What factors determine cation coordination numbers? *Acta Crystallogr B* 44(6):545–553.
34. Villegas-Jiménez A, Mucci A, Whitehead MA (2009) Theoretical insights into the hydrated (10.4) calcite surface: Structure, energetics, and bonding relationships. *Langmuir* 25(12):6813–6824.
35. Radha AV, Navrotsky A (2013) Thermodynamics of carbonates. *Rev Mineral Geochem* 77(1):73–121.
36. Bruno M, et al. (2013) New estimates of the free energy of calcite/water interfaces for evaluating the equilibrium shape and nucleation mechanisms. *Cryst Growth Des* 13(3):1170–1179.
37. Balluffi RW, Allen S, Craig Carter W (2005) *Kinetics of Materials* (Wiley Interscience, Hoboken, NJ).
38. Morse JW, He S (1993) Influences of *T, S* and P_{CO2} on the pseudo-homogeneous precipitation of $CaCO_3$ from seawater: Implications for whiting formation. *Mar Chem* 41(4):291–297.
39. Wallace AF, et al. (2013) Microscopic evidence for liquid-liquid separation in supersaturated CaCO3 solutions. *Science* 341(6148):885–889.
40. Gebauer D, Völkel A, Cölfen H (2008) Stable prenucleation calcium carbonate clusters. *Science* 322(5909):1819–1822.
41. Demichelis R, Raiteri P, Gale JD, Quigley D, Gebauer D (2011) Stable prenucleation mineral clusters are liquid-like ionic polymers. *Nat Commun* 2:590.
42. Bots P, Benning LG, Rodriguez-Blanco J-D, Roncal-Herrero T, Shaw S (2012) Mechanistic insights into the crystallization of amorphous calcium carbonate (ACC). *Cryst Growth Des* 12(7):3806–3814.
43. Radha AV, Forbes TZ, Killian CE, Gilbert PU, Navrotsky A (2010) Transformation and crystallization energetics of synthetic and biogenic amorphous calcium carbonate. *Proc Natl Acad Sci USA* 107(38):16438–16443.
44. Kabalah-Amitai L, et al. (2013) Vaterite crystals contain two interspersed crystal structures. *Science* 340(6131):454–457.
45. Demichelis R, et al. (2013) The multiple structures of vaterite. *Cryst Growth Des* 13(6): 2247–2251.
46. Belcher AM, et al. (1996) Control of crystal phase switching and orientation by soluble mollusc-shell proteins. *Nature* 381:56–58.
47. Falini G, Albeck S, Weiner S, Addadi L (1996) Control of aragonite or calcite polymorphism by mollusk shell macromolecules. *Science* 271(5245):67–69.
48. Giuffre AJ, Hamm LM, Han N, De Yoreo JJ, Dove PM (2013) Polysaccharide chemistry regulates kinetics of calcite nucleation through competition of interfacial energies. *Proc Natl Acad Sci USA* 110(23):9261–9266.
49. Teng HH, Dove PM, Orme CA, De Yoreo JJ (1998) Thermodynamics of calcite growth: Baseline for understanding biomineral formation. *Science* 282(5389):724–727.
50. Han Y-J, Wysocki LM, Thanawala MS, Siegrist T, Aizenberg J (2005) Template-dependent morphogenesis of oriented calcite crystals in the presence of magnesium ions. *Angew Chem Int Ed Engl* 44(16):2386–2390.
51. Smeets PJM, Cho KR, Kempen RGE, Sommerdijk NAJM, De Yoreo JJ (2015) Calcium carbonate nucleation driven by ion binding in a biomimetic matrix revealed by in situ electron microscopy. *Nat Mater* (January):26.
52. Verch A, Antonietti M, Cölfen H (2012) Mixed calcium-magnesium pre-nucleation clusters enrich calcium. *Z Krist - Cryst Mat* 227(11):718–722.
53. Bentov S, Weil S, Glazer L, Sagi A, Berman A (2010) Stabilization of amorphous calcium carbonate by phosphate rich organic matrix proteins and by single phosphoamino acids. *J Struct Biol* 171(2):207–215.
54. Kresse G, Furthmüller J (1996) Efficient iterative schemes for ab initio total-energy calculations using a plane-wave basis set. *Phys Rev B Condens Matter* 54(16): 11169–11186.
55. Kresse G, Joubert (1999) From ultrasoft pseudopotentials to the projector augmented-wave method. *Phys Rev B* 59(3):1758.
56. Perdew JP, Burke K, Ernzerhof M (1996) Generalized gradient approximation made simple. *Phys Rev Lett* 77(18):3865–3868.
57. Ong SP, et al. (2013) Python Materials Genomics (pymatgen): A robust, open-source python library for materials analysis. *Comput Mater Sci* 68:314–319.